Vibrational−Rotational Energy Distributions in the Reaction $O^- + D_2 \rightarrow OD + D^-$†

Yue Li,‡ Li Liu,§ and James M. Farrar*

Department of Chemistry, University of Rochester, Rochester, New York 14627

Received: June 15, 2009; Revised Manuscript Received: September 28, 2009

The D^+ transfer reaction between O^- (^2P) and D_2 to form OD and D^- was studied using the crossed molecular beam technique at collision energies of 1.55 and 1.95 eV. The reaction appears to proceed by a direct mechanism through large impact parameters. At both collision energies, more that 70% of the excess energy is partitioned into product translation. At the lower collision energy, the OD products are formed in the ground vibrational state with a bimodal rotational energy distribution. At the higher collision energy, both $v' = 0$ and 1 products are formed; ground vibrational state products have a mean rotational energy of 0.05 eV, corresponding to $J' \approx 6$. In contrast, OD products formed in $v' = 1$ are formed with significant rotational excitation, with the most probable $J' \approx 15$. The bimodal rotational distribution is rationalized in terms of trajectories that sample two potential surfaces coupled by a conical intersection in the vicinity of the $[O\cdots DD]^-$ intermediate that correlate to (OD^-,D) or (OD,D^-) products.

I. Introduction

The reaction of O^- with the hydrogen molecule and its isotopomers is one of the simplest anion-neutral systems and has been studied theoretically[1] and experimentally.[2−6] Owing to its apparent simplicity, the system is an ideal model for computing accurate potential energy surfaces for anionic systems and testing dynamical theories on those potential energy surfaces. At low collision energies, the system has two exoergic channels corresponding to associative detachment (AD) and hydrogen atom transfer, channels 1 and 2, respectively, and endoergic proton transfer, reaction 3, shown as follows

$$O^- + H_2 \rightarrow H_2O + e^- \quad \Delta H = -3.60\ \text{eV} \qquad (1)$$

$$\rightarrow OH^- + H \quad \Delta H = -0.30\ \text{eV} \qquad (2)$$

$$\rightarrow H^- + OH \quad \Delta H = +0.79\ \text{eV} \qquad (3)$$

Channels 1 and 2 have received significant attention, but the endoergic proton transfer reaction, channel 3, has been studied in much less detail. This article presents a product state-resolved crossed beam study of this channel at collision energies of 1.55 and 1.95 eV.

Drift tube experiments over the energy range from thermal to 0.9 eV probed only the exoergic channels[3,7,8] and showed that associative detachment (reaction 1) is the predominant process, especially at low collision energies. At 300 K, the branching ratio of associative detachment to hydrogen atom transfer is 0.96:0.04 (0.98:0.02 for the deuterium system). With increasing collision energy, the rate of the associative detachment reaction decreases sharply, but the rapid increase in the particle transfer process rate leads to a weak dependence of the total rate of O^- destruction in the energy range from thermal to 0.9 eV.

Mauer and Schulz[9] employed an ion beam−gas cell geometry to study the associative detachment reaction of O^- with H_2 in the collision energy range up to 10 eV. By measuring the kinetic energy distribution of the detached electrons, the internal energy distribution of the H_2O product was determined. Their results showed that H_2O was formed with high vibrational excitation, primarily in the bending mode, accounting for nearly 75% of the available energy. In a related experiment employing an ion beam impinging on an effusive beam of H_2, Esaulov et al.[10] also found that the associative detachment reaction leads to highly rovibrationally excited H_2O molecules. However, they did not observe any significant structure that could be assigned to the excitation of specific vibrational modes.

The hydrogen (deuterium) transfer channel to form OH^- (OD^-) has been studied with crossed-molecular beams[4−6,11−13] and ion beam−gas cell scattering techniques[14−16] at relative collision energies up to 14 eV. The latter experiments yielded estimates of total cross sections[14] and provided evidence of the hydrogen atom transfer process being direct.[15,16] The crossed beam results at relative collision energies below 2.5 eV obtained by Johnson et al.[12] were consistent with the formation of highly internally excited OD^- products but suggested that the reaction proceeds through a transient complex living approximately a rotational period. Higher-resolution vibrational state-resolved measurements from our laboratory[4,11,13] confirmed the high internal excitation in the products but provided clear evidence that the reaction proceeds in a direct manner down to 0.5 eV, with the time scale of the reaction only approaching that of a rotational period at energies below 0.37 eV. Our laboratory results[6] also showed that D_2 rotational excitation strongly affects the product angular distribution. The data suggested that correlation of D_2 rotational motion with the bending modes in the $[OD\cdots D]^-$ intermediate and transition state selectively control the branching between electron detachment and D-atom transfer.

Many fewer results have been reported on the endothermic H^- (or D^-) channel. The beam-gas experiments of Esaulov et al.[10] measured the kinetic energy distribution of the H^- product ions formed by proton transfer in the collision energy range from 1 to 10 eV. They found that the H^- energy distributions

† Part of the "Vincenzo Aquilanti Festschrift".

* To whom correspondence should be addressed. E-mail: farrar@chem.rochester.edu.

‡ Present address: Department of Chemistry, University of Maryland, College Park, MD 20742.

§ Present address: 94 Oxford Street, Coalville, LE67 3GR, U.K.

10.1021/jp905610u
Published on Web 10/16/2009

were structured and suggested that the OH products were vibrationally excited. Huq et al.[17] also determined absolute total cross sections for electron detachment and H^- (D^-) production for collisions of O^- with H_2 and D_2 for relative collision energies ranging from 0.5 to 25 eV.

Electron impact on H_2O also probes the $[H_2O]^-$ potential surface, and early experiments[18,19] reported on the production of H^- (D^-) ions by dissociative attachment (DA). Later experiments[20−25] demonstrated that the negative ion resonance states of water play a dominant role in the production of H^-, O^-, and OH^- ions. Of particular interest was the fact that the H^- energy distributions[25] formed by DA closely resembled the ones observed in the proton transfer experiments of Esaulov et al.,[10] suggesting that both processes probe common regions of the $[H_2O]^-$ potential energy surface. Measurements of the angular distributions of the fragment negative ions[25] have indicated that the symmetries of the three lowest-lying resonance states of H_2O^- are $^2B_1$, $^2A_1$, and $^2B_2$ (located at 6.5, 8.6, and 11.8 eV), respectively, in which the $^2B_1$ state dominates the DA processes forming H^-, O^-, and OH^-.[20]

Theoretical calculations[26−28] on the $[H_2O]^-$ surface have been directed primarily toward addressing the nature of the binding of the excess electron by the dipole of H_2O. Early approximate MO calculations[29] were carried out in the vicinity of the electron continuum corresponding to $H_2O + e^-$. A more recent ab initio calculation by Werner et al.[1] focused on the stability of the $[H_2O]^-$ anion, detected in mass spectrometry by Nibbering and coworkers.[30] The calculations showed that approaching $O^- + H_2$ reactants form two states ($^2\Sigma$ and $^2\Pi$) in $C_{\infty v}$ symmetry, depending on the orientation of the 2p orbital in which the unpaired electron resides relative to the plane of the atoms. Both of these entrance channel surfaces are attractive, with the $^2\Pi$ state lying lower in energy. The $^2\Pi$ surface correlates to the H^- ionic product, whereas the $^2\Sigma^+$ surface leads to the OH^- ionic product. Both of the surfaces have shallow minima that correspond to complexes characterized as O^- bound to D_2 in a collinear configuration by the ion-quadrupole interaction. Deuterium transfer to oxygen leads to complexes corresponding to the $[OD\cdots D]^-$ structure. In the vicinity of this deuterium transfer, the surfaces experience a conical intersection that plays a role in the formation of the $OD^- + D$ or $OD + D^-$ products.

This article reports crossed molecular beam measurements results of the D^- channel of the $O^- + D_2$ reaction at the two collision energies, 1.55 and 1.95 eV. These two energies are close to 2.5 eV, where the cross section for H^- (D^-) production reaches a maximum.[17] The angular and kinetic energy distributions of the D^- ions are obtained for the first time. The reaction kinematics constrain the D^- velocity distributions to encode the OD internal state populations with high resolution, providing a detailed look at the reaction dynamics. Of particular interest in this study is the fact that the kinetic energy distributions reveal information on the rotational energy of the OD products. The key role that rotational energy partitioning plays in elucidating the dynamics of light atom transfer reactions, particularly involving hydrogen atoms, has been noted in a number of reports and review articles.[31−34] In this study, we argue that the product rotational energy distributions are bimodal at the lowest collision energy and provide clear evidence for the participation of two potential energy surfaces in product formation.

II. Experimental Section

The experimental apparatus has been described in detail in previous publications,[35] so only a brief overview is provided here. The O^- ions were produced by electron impact on N_2O (99.6% purity) gas. The pressure in the ion source was typically 0.01 Torr. The ions were mass-selected with a 60° magnetic sector. After deceleration to the desired beam energy and focusing by a series of ion optics, the beam had a laboratory kinetic energy distribution with fwhm of ∼0.25 eV. The O^- beam laboratory energies of 7.4 and 9.4 ± 0.12 eV correspond to center of mass energies of 1.55 and 1.95 ± 0.03 eV. The indicated uncertainties correspond to fwhm values.

The deuterium beam was formed by supersonic expansion of the pure gas through a 0.07 mm nozzle. A 1.0 mm diameter skimmer, located 50 nozzle diameters downstream from the nozzle, selected the cool core of the beam. The beam entered a differential pumping chamber, where it was collimated with a 3.0 mm square aperture located ∼2.5 cm from the skimmer before entering the main chamber, where it intersected the ion beam at a 90° angle. A tuning fork chopper modulated the beam at 30 Hz to provide the synchronization for the experiment. The most probable velocity of the neutral beam formed through supersonic expansion was calculated using eq 4

$$V_{\text{peak}} = \sqrt{\frac{2kT}{m}\left(\frac{\gamma}{\gamma - 1}\right)} \tag{4}$$

in which γ, the ratio of heat capacities, is 1.4 for D_2.

Both reactant ions and scattered product ions were energy-analyzed with a 90° spherical sector electrostatic deflector analyzer with laboratory resolution of 0.07 eV. The ions were then mass-analyzed with a quadrupole mass spectrometer and detected with a dual microchannel plate ion detector. The entire detector was rotatable in the plane of the beams over a range of lab angles from −2 to +110° relative to the direction of the primary ion beam. Data were collected with a computer-controlled multichannel scalar synchronized with the beam modulation.

Because the experiments require accurate and precise measurements of the energy distributions of low energy ions, the energy analyzer was calibrated before and after each experiment. The resonant charge transfer reaction between NO^- and NO was used as the calibration reaction to determine the zero offset of the energy analyzer.

In the experiments, two independent measurements were performed. First, by rotating the angle of the detector, the relative angular distribution of product ions in the laboratory coordinate system was measured. Second, the kinetic energy distributions of the product ions at 22 fixed laboratory angles were measured. Each energy spectrum consists of 80 points, with typical energy bin widths of 0.025 eV. As noted in the next section, determining reliable center of mass distributions, especially internal state-resolved kinetic energy distributions, is critically dependent on normalizing kinetic energy scans at fixed lab scattering angles to the lab angular distribution. Care was taken to ensure that lab angular distribution intensities were precise to well within 5% standard deviation. The two measurements result in data sets consisting of ∼1800 data points covering laboratory velocity space.

III. Data Analysis

The experimental results measured in the laboratory coordinate system were transformed to center of mass (c.m.) coordinates to obtain c.m. reaction differential cross sections, $I_{\text{c.m.}}(u,\theta)$. In the experiments, the reactant ion and neutral beams had velocity and angular spreads that resulted in distributions of collision energies and intersection angles. In the coordinate

transformation and data analysis, these distributions were taken into account.

The experimental data, in the form of fluxes at constant increments in lab energy, were preconditioned numerically before being transformed. The preconditioning procedure first deconvoluted the 0.07 eV wide triangular energy bandpass function of the energy analyzer and then interpolated among the data points to produce a data set at constant increments in lab velocity. The data points were then analyzed by the deconvolution routine, which unfolded the distribution of lab velocities while transforming the data to center of mass coordinates. This procedure was accomplished with a pointwise iterative deconvolution procedure using eq 5 as developed by Siska[36]

$$I_{\mathrm{lab}}(v,\Theta) = \sum_{i=1}^{N} f_i \frac{v^2}{\mathrm{u}_i^2} I_{\mathrm{c.m.}}(\mathrm{u}_i,\theta_i) \qquad (5)$$

In practical calculations, five points were used to represent the energy distributions of each of the two reagent beams, and five points represented the intersection angle distribution; thus, in the above equation, N is 125. The quantities f_i are weighting factors that represented the probability of observing the ith Newton diagram based on the reagent beam distributions. The comparison between the simulated and experimental results provided a figure of merit for the deconvolution process. In this study, the standard deviations of the simulations were <10%.

Using the derived $I_{\mathrm{c.m.}}(\mathrm{u},\theta)$, the barycentric angular distribution, $g(\theta)$, of the products can be calculated by integrating over product translational energy. The angular distribution $g(\theta)$ represents the relative intensities of products scattered into c.m. scattering angle θ averaged over product kinetic energy. In practice, it was calculated by replacing the integral with a summation

$$g(\theta) = \sum_{i}^{M} I_{\mathrm{c.m.}}(\mathrm{u}_i,\theta) \qquad (6)$$

Similarly, the angle-averaged relative translational energy distribution of products, $P(E_T')$, was calculated using eq 7.

$$P(E_T') = \sum_{\mathrm{i}}^{L} I_{\mathrm{c.m.}}(\mathrm{u},\theta_i)\frac{\sin\theta_i}{\mathrm{u}} \qquad (7)$$

The indices L and M control the grid on which the summations are performed and are varied, within the constraints of the size of the data set, to ensure that the calculated distributions are smooth.

The accuracy and precision of the angular and energy distributions are clearly determined by the signal-to-noise ratio of the data, primarily arising from counting statistics but also by the experimental grid on which the data are obtained. Because the product flux is distributed sharply along the relative velocity vector, the lab angular distribution grid is the most important determinant of the normalization and spacing of data points along the relative velocity vector. In the collision energy range of the experiments reported here, a spacing of 5° in lab coordinates corresponds to an increment of 0.02 eV in relative kinetic energy directed along the relative velocity vector. In the present experiments, the accuracy and precision of the lab angular distributions constrain their maxima to an angular range of no more than 5°. We conservatively estimate that the most probable relative kinetic energies of products are known with an uncertainty of no more than ±0.015 eV.

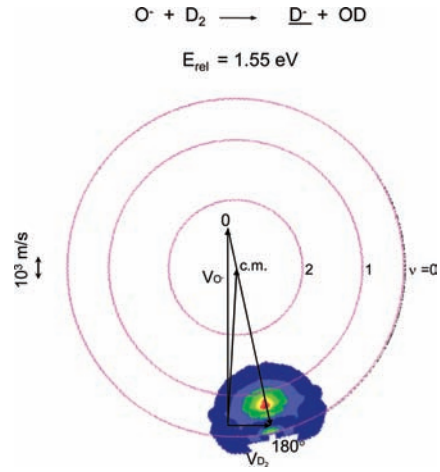

Figure 1. Newton diagram and scattered product flux contour map at the collision energy of 1.55 eV.

IV. Results and Discussion

Kinetic energy distributions of product D^- ions were measured at c.m. collision energies of 1.55 and 1.95 eV. The corresponding primary ion beam energies were 7.40 and 9.41 eV, respectively. In the experiments, we determined the branching ratio of the two products OD^-/D^-, performed by direct integration of product signals, to be approximately 2:1 at the collision energy of 1.95 eV. Unlike the OD^- product ions, which are distributed over a small angular range in the lab from 0 to 10°, the D^- ion distribution extends over the entire range of lab angles, from −2 to 112°. Experimentally, this results in a weak signal for the D^- ions at each angle but improves the kinematic dispersion, allowing the internal state distributions of the correlated OD products to be encoded in the D^- velocity distributions with high resolution. Plots of selected experimental data, including lab fluxes at fixed laboratory angles, the lab angular distribution used for normalization of the data, and the fits provided by the iterative deconvolution procedure, are shown in the Supporting Information for this article.

Figure 1 shows the contour map of the D^- product ion center of mass flux at the relative energy of 1.55 eV, also obtained by deconvolution. The contour map is superimposed on the Newton diagram in the Figure. The angular and kinetic energy distributions obtained by integration of the c.m. flux using eqs 6 and 7 are shown in Figure 2. Figure 2a shows that the distribution of the D^- product ions is asymmetric, and most products appear at large angles, that is, close to the direction of the precursor D_2 beam, corresponding to forward scattering. By convention, 0° in c.m. coordinates corresponds to the direction of the ion beam. According to momentum conservation, its neutral partner, OD, is mainly scattered in the direction of the primary ion beam, O^-. This observation indicates that the reaction proceeds as a direct process and through large impact parameters. The data provide no evidence of an $[ODD]^-$ intermediate living a significant fraction of a rotational period.

As noted in the Results and Discussion section, precise normalization of the fluxes to the lab angular distribution is critical in extracting reliable product state distributions. Because of the reaction kinematics as well as dynamical features that form products sharply distributed along the relative velocity

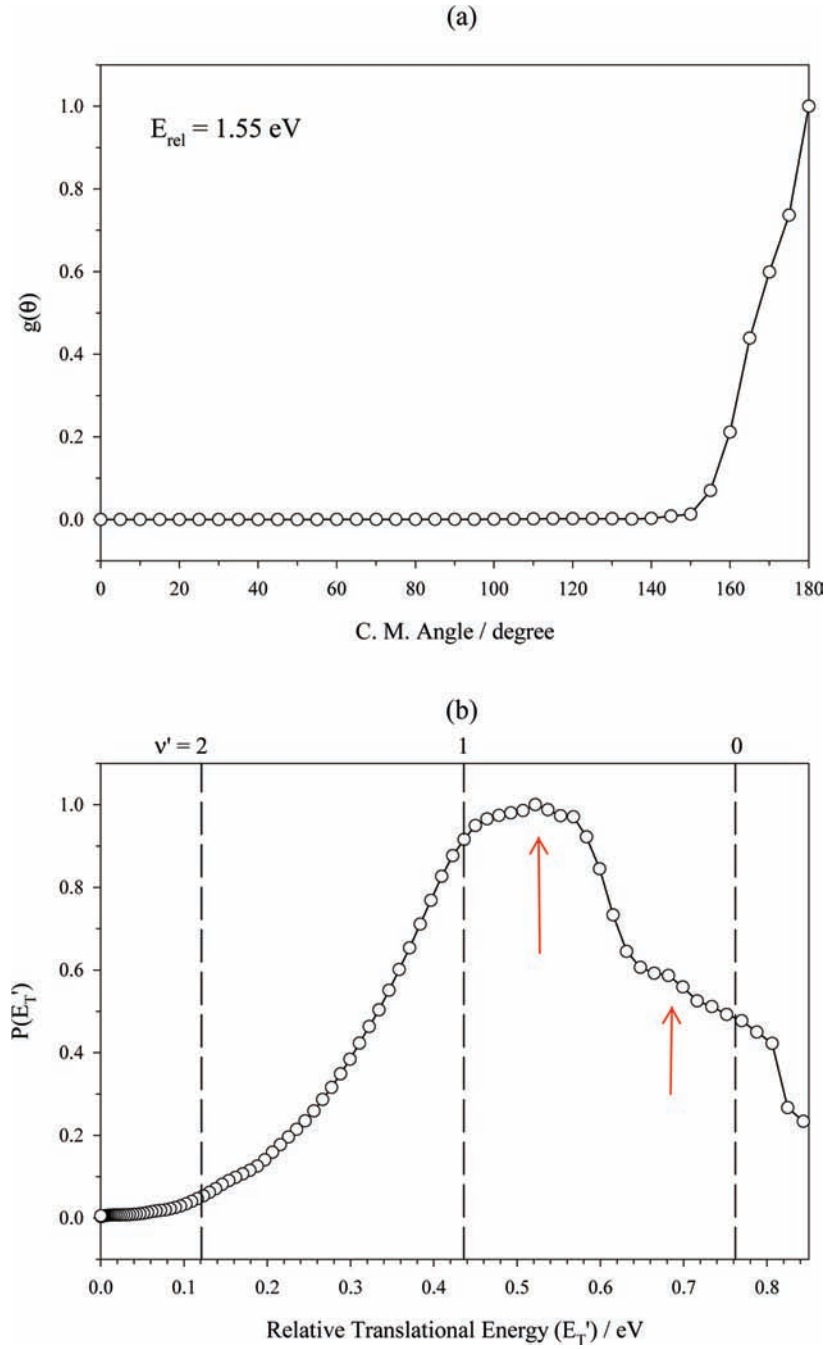

Figure 2. (a) Angular distributions; (b) relative translational energy distributions of the products in c.m. coordinates at the collision energy of 1.55 eV. The internal energy of the OD products increases right to left from the thermochemical limit at 0.76 eV. Vertical arrows denote the position of the most probable rotational energies for ground vibrational state products.

vector, kinetic energy scans at a given lab angle will intersect the flux from only a single vibrational state. The lab scattering angle must be varied to probe flux correlated with different vibrational states, making a precise determination of the lab angular distribution critical. That point comes into play in the discussion of the kinetic energy distributions in the following paragraphs.

Figure 2b shows the kinetic energy distribution of the products. The internal energies of OD products increase right to left on this plot, and the thresholds for particular vibrational energy states are indicated along the top axis. Energy conservation allows us to assign specific ranges of relative energies over which OD products in particular internal energy states are formed, and those are shown in Figure 2b. The vertical dashed lines indicate the relative kinetic energies corresponding to the formation of OD products in specific vibrational levels without any rotational energy. The OD vibrational and rotational parameters are taken from the literature.[37] The Figure shows that the kinetic energy distribution spills over the thermochemical limit by ~0.05 eV. This small amount of spill reflects low signal levels at the low lab energies where these products appear, imperfections in the deconvolution procedure, arising from neglecting the unknown dependence of the cross section on relative energy, and from the finite angular resolution of the detector, which at large laboratory scattering angles introduces broadening in the distribution of the highest kinetic energy products. As we noted in the Data Analysis section, the most probable product kinetic energies are determined with an uncertainty of ±0.015 eV.

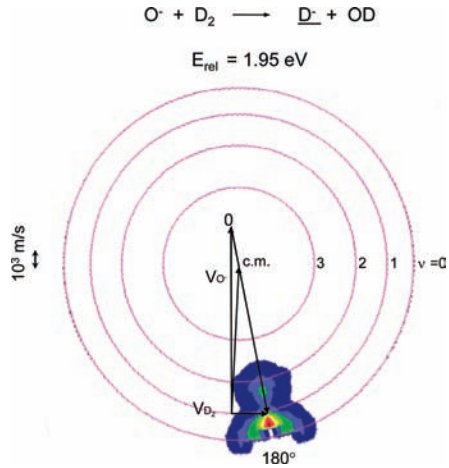

Figure 3. Newton diagram and scattered product flux contour map at the collision energy of 1.95 eV.

The kinetic energy distribution shown in Figure 2b has a broad peak centered at 0.52 eV and a shoulder that extends to the thermochemical limit at 0.76 eV. Those two features occur in the range of kinetic energies that corresponds to the formation of the OD product in the ground vibrational state. A significant tail in the distribution to lower kinetic energies suggests that higher vibrational states may be populated, but we are unable to state definitively whether those products are formed in the $v' = 1$ state. The distribution shows an inflection point at 0.62 eV, 0.18 eV above the maximum kinetic energy of $v' = 1$, $J' = 0$ products. Because this inflection point is displaced by at least three times the energy uncertainty created by the spill past the thermochemical limit, we are comfortable in assigning both features above a translational energy of 0.44 eV to ground vibrational state products. We conclude that the distribution of rotational states in the ground vibrational state of OD is bimodal. The most probable rotational energy of the low energy peak is ~0.08 eV (i.e., the most probable energy appears at a translational energy ~0.08 eV below the thermochemical limit at 0.76 eV), corresponding to $J' \approx 8$, and the most probable value of the higher rotational energy band is ~0.24 eV, corresponding to $J' \approx 14$.

Although the kinetic energy distribution extends into the range where products in the first excited vibrational state may be formed, the distribution is smooth and does not show any structure at the $v' = 1$ threshold. The data do not allow a distinction between highly rotationally excited OD molecules formed in $v' = 0$ and rotationally cold molecules formed in $v' = 1$; however, the smoothness of the energy distribution is consistent with excitation of a continuous distribution of product rotations extending to high J'. A simple integration of the distribution over appropriate ranges of energies establishes the lower bound on the fraction of products formed in the ground state at 70%. The average product kinetic energy is 0.54 eV, corresponding to 71% of the total available energy.

The results for the 1.95 eV collision energy experiment are shown in Figures 3 and 4. The flux distribution shown in Figure 3 is qualitatively similar to the lower energy plot and shows that the D^- angular distribution is also sharply asymmetric and strongly forward scattered. The structure corresponding to discrete vibrational states is more apparent in the higher-energy experiment.

Figure 4a shows the product angular distribution evaluated by integration over c.m. speed, and the lower panel of the Figure shows the product kinetic energy distribution. The distribution

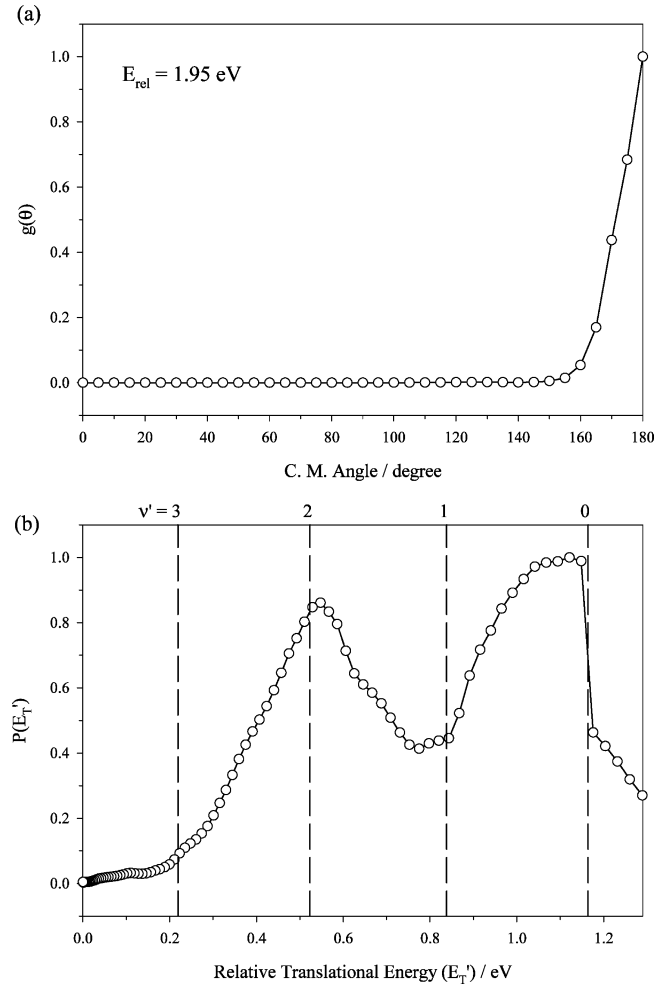

Figure 4. (a) Angular distribution; (b) relative translational energy distribution of the products in c.m. coordinates at the collision energy of 1.95 eV.

exhibits a sharp cutoff at 1.16 eV, the thermochemical limit, although there is a weak shoulder at higher energies. Consistent with the more structured flux distribution in Figure 3, the kinetic energy distribution in Figure 4b shows a well-resolved peak at ~1.10 eV associated with products formed in $v' = 0$, formed with low rotational excitation. A second peak at 0.55 eV corresponds to highly rotationally excited products formed in $v' = 1$. The tail of this distribution extends smoothly to lower kinetic energies where products may correspond to OD formed in $v' = 2$, but as was the case at the lower collision energy, the data do not allow us to distinguish molecules formed in $v' = 2$ or high J' states in $v' = 1$. There is some evidence of a shoulder in the data between 0.6 and 0.7 eV that might correspond to the formation of $v' = 1$ molecules with lower rotational excitation, but the data do not warrant fitting a more structured distribution to them. According to the previous discussion, the most probable rotational energy for ground vibrational state products is ~0.05 eV ($J' \approx 6$), whereas the most probable rotational energy for $v' = 1$ products is 0.27 eV ($J' \approx 15$).

The magnitudes of the rotational quantum numbers are consistent with angular momentum conservation. The measured absolute total cross section for D^- production[17] at 1.5 eV is 2.2 Å^2, producing a value for the initial orbital angular momentum of ~24 $\hbar$. D_2 reactants prepared by supersonic expansion are rotationally cold and do not contribute significantly to the total angular momentum. The partitioning of the total angular momentum into significant rotational excitation is consistent

with the product translational energies, the two-fold decrease in reduced mass upon reaction, and the range of the exit channel potential energy.

The kinetic energy distribution for product formation at 1.95 eV yields a mean value for product translational energy of 0.32 eV, corresponding to 72% of the available energy. Therefore, the fraction of the available energy appearing in product translation is essentially energy independent. The fact that reactant translational energy is preferentially partitioned into product translation is consistent with the fact that the barrier in this endoergic reaction occurs very close to the position of the products. This result is qualitatively consistent with the measurement of Esaulov et al.,[10] who found that the OH products are formed predominantly in the vibrational ground state at low energies but with a modest increase in vibrational excitation with increasing collision energy.

The D^- channel in the well-studied $O^- + D_2$ system presents a number of surprises. First of all, the endoergic process proceeds through large impact parameters, exhibiting behavior qualitatively similar to "stripping" dynamics. Although examples of endoergic stripping are known in the literature, they predict a single, sharp velocity at which products are formed.[38] The appearance of a distribution of product states argues against such a simple mechanism. Second, the formation of ground vibrational state products with a bimodal rotational state distribution suggests that the collision dynamics cannot be characterized via a simple direct particle transfer reaction. Finally, at the higher collision energy, where both $v' = 0$ and 1 OD vibrational states are formed, the rotational energy in the vibrationally excited state is significantly higher than that in the ground state. This result is in apparent conflict with the constraints of conservation of energy and angular momentum.

There are a number of reports of simple chemical reactions in which the dynamics produce bimodal rotational distributions. The well-studied $F + H_2$ reaction produces bimodal rotational distributions that are thought to be associated with dynamical resonances.[39−42] The possibility of multiple collisions, in which O^- first collides with the first D atom, retreats nonreactively, and then reacts with the second D atom, an idea advanced by Polanyi[43] early in the history of molecular reaction dynamics, may also provide a plausible explanation for this behavior. Another important mechanism for producing bimodal rotational distributions is the participation of more than one electronic potential energy curve/surface, such that each branch of the rotational distribution is governed by motion on different potential curves.[44,45] There are features of the $O^- + D_2$ system that suggest the plausibility of such a mechanism in the present system. In the entrance channel, the orientation of the p orbital on O^- containing the unpaired electron determines whether the system follows the $\Sigma(A')$ or $\Pi(A',A'')$ potential energy surface. In the entrance channel and in the vicinity of the initial electrostatically bound species denoted $[O\cdots DD]^-$, the Π surface lies lower in energy, but in the region where deuterium transfer to oxygen occurs, the surfaces undergo a conical intersection. Along one surface, a deuterium ion has been transferred, and along the other, a deuterium atom has been transferred to oxygen. Therefore, the surface interaction occurs between two states related by a single electron transfer. The nature of the interacting states opens up the possibility that one branch of the rotational distribution arises from products evolving on one surface only, whereas the second branch is associated with products formed after undergoing electron transfer. The nature of these interactions also plays a role in determining the branching ratio for hydrogen atom transfer to proton transfer. These are issues that require additional theoretical investigation.

The partitioning of rotational energy as a function of vibrational state is also surprising. At the higher collision energy, the most probable product rotational energy in $v' = 0$ is 0.05 eV ($J' \approx 6$), but is more than five times higher (0.27 eV) in $v' = 1$, corresponding to $J' \approx 15$. Simultaneous conservation of energy and angular momentum generally constrains vibrational and rotational energies to be anticorrelated. However, Valentini and coworkers[31−33] made related observations in hydrogen atom abstraction reactions from the polyatomic molecules $CHCl_3$, *n*-pentane, and *n*-hexane to form H_2. These investigators observed the same positive correlation of vibrational and rotational energy in H_2, the effect increasing with the complexity of the molecular fragment produced in concert with H_2. The argument was advanced that the constraints of simultaneous conservation of energy and angular momentum could be relaxed by the ability of the polyatomic fragment to dispose of angular momentum in its rotational degrees of freedom. However, that mechanism is not applicable in the $O^- + D_2$ case because OD is accompanied by an atomic ion product with no ability to acquire rotational angular momentum. The origin of this positive correlation of vibrational and rotational energy remains unclear. It is interesting, however, to reflect on the fact that unlike many chemical reactions in which details of the dynamics can be inferred from product vibrational distributions, this reaction yields dynamical insight from the product rotational energy distributions. Angular momentum encodes information on reactant and product masses, relative velocities, and the length scale of the entrance and exit channel interactions and therefore has high information content. In the present case, the data are capable of revealing this information content, confirming the claim made by Valentini in a 2002 review on state-to-state reaction dynamics studies that "rotations tell the tale."[34]

V. Conclusions

The study of the D^- production channel in the $O^- + D_2$ system adds to the richness of the dynamics of this already complex collision process. Like the exoergic channel to form OD^-, the D^- channel proceeds via a direct mechanism in which the center-of-mass flux distributions of the D^- ions exhibit sharp asymmetry, with the maxima close to the velocity and direction of the precursor D_2 beam. However, the endoergic process partitions over 70% of the available energy into product translation. Perhaps the most interesting observation concerns the partitioning of angular momentum in the reaction products. At the lower collision energy of 1.55 eV, 0.76 eV above the reaction threshold, the distribution of rotational energy in the ground vibrational state products is bimodal, with peaks near $J' = 8$ and 14. We speculate that this bimodal character may arise from trajectories that sample two potential surfaces coupled by a conical intersection in the vicinity of the $[O\cdots DD]^-$ intermediate that correlate to (OD^-,D) or (OD,D^-) products. Finally, at the higher collision energy of 1.95 eV, the ground vibrational state products have low rotational excitation with $J' \approx 6$, whereas products formed in $v' = 1$ show a rotational distribution sharply peaked near $J' = 15$.

It is clear that additional theoretical work will be necessary to unravel the nature of the product rotational energy partitioning in the formation of D^- products. We look forward to those studies.

Acknowledgment. We are grateful to the U.S. Department of Energy for partial support of this work. We thank Scott

Martin and Xiaohui Cai for their assistance with the data collection and reduction.

Supporting Information Available: Plots of lab fluxes at fixed laboratory angles and the fits provided by the iterative deconvolution procedure. This material is available free of charge via the Internet at http://pubs.acs.org.

References and Notes

(1) Werner, H.-J.; Mänz, U.; Rosmus, P. *J. Chem. Phys.* **1987**, *87*, 2913.
(2) Hauffe, B. J. *Z. Phys. Chem.* **1973**, *85*, 175.
(3) Viggiano, A. A.; Morris, R. A.; Deakyne, C. A.; Dale, F.; Paulson, J. F. *J. Phys. Chem.* **1991**, *95*, 3644.
(4) Carpenter, M. A.; Farrar, J. M. *J. Phys. Chem. A* **1997**, *101*, 6870.
(5) Lee, S. T.; Farrar, J. M. *J. Chem. Phys.* **1999**, *111*, 7348.
(6) Lee, S. T.; O'Grady, E. R.; Carpenter, M. A.; Farrar, J. M. *Phys. Chem. Chem. Phys.* **2000**, *2*, 679.
(7) Parkes, D. A. *J. Chem. Soc., Faraday Trans. 1* **1972**, *68*, 613.
(8) McFarland, M.; Albritton, D. L.; Fehsenfeld, F. C.; Ferguson, E. E.; Schmeltekopf, A. L. *J. Chem. Phys.* **1973**, *59*, 6629.
(9) Mauer, J. L.; Schulz, G. J. *Phys. Rev. A* **1973**, *7*, 593.
(10) Esaulov, V. A.; Champion, R. L.; Grouard, J. P.; Hall, R. I.; Montmagnon, J. L.; Penent, F. *J. Chem. Phys.* **1990**, *92*, 2305.
(11) Carpenter, M. A.; Farrar, J. M. *J. Phys. Chem. A* **1997**, *101*, 6475.
(12) Johnson, S. G.; Kremer, L. N.; Metral, C. J.; Cross, R. J. *J. Chem. Phys.* **1978**, *68*, 1444.
(13) Carpenter, M. A.; Zanni, M. T.; Farrar, J. M. *J. Phys. Chem.* **1995**, *99*, 1380.
(14) Martin, J. D.; Bailey, T. L. *J. Chem. Phys.* **1968**, *49*, 1977.
(15) Doverspike, L. D.; Champion, R. L.; Lam, S. K. *J. Chem. Phys.* **1973**, *58*, 1248.
(16) Herbst, E.; Payne, L. G.; Champion, R. L.; Doverspike, L. D. *Chem. Phys.* **1979**, *42*, 413.
(17) Huq, M. S.; Scott, D.; Champion, R. L.; Doverspike, L. D. *J. Chem. Phys.* **1985**, *82*, 3118.
(18) Lozier, W. W. *Phys. Rev.* **1930**, *36*, 1417.
(19) Schulz, G. J. *J. Chem. Phys.* **1960**, *33*, 1661.
(20) Seng, G.; Linder, F. *J. Phys. B: At., Mol. Opt. Phys.* **1976**, *9*, 2539.
(21) Keough, T.; Beynon, J. H.; Cooks, R. G. *Chem. Phys.* **1976**, *12*, 191.
(22) Jungen, M.; Vogt, J.; Staemmler, V. *Chem. Phys.* **1979**, *37*, 49.
(23) Melton, C. E. *J. Chem. Phys.* **1972**, *57*, 4218.
(24) Trajmar, S.; Hall, R. I. *J. Phys. B: At., Mol. Opt. Phys.* **1974**, *7*, L458.
(25) Belic, D. S.; Landau, M.; Hall, R. I. *J. Phys. B: At., Mol. Opt. Phys.* **1981**, *14*, 175.
(26) Weiss, A. W.; Krauss, M. *J. Chem. Phys.* **1970**, *52*, 4363.
(27) Winter, N. W.; Goddard, W. A. I.; Bobrowicz, F. W. *J. Chem. Phys.* **1975**, *62*, 4325.
(28) Burke, P. G.; Chandra, N.; Gianturco, F. A. *J. Phys. B: At., Mol. Opt. Phys.* **1972**, *5*, 2212.
(29) Claydon, C. R.; Segal, G. A.; Taylor, H. S. *J. Chem. Phys.* **1971**, *54*, 3799.
(30) de Koning, L. J.; Nibbering, N. M. M. *J. Am. Chem. Soc.* **1984**, *106*, 7971.
(31) Lanzisera, D. V.; Valentini, J. J. *Chem. Phys. Lett.* **1993**, *216*, 122.
(32) Lanzisera, D. V.; Valentini, J. J. *J. Chem. Phys.* **1994**, *101*, 1165.
(33) Picconatto, C. A.; Srivastava, A.; Valentini, J. J. *J. Chem. Phys.* **2001**, *114*, 4837.
(34) Valentini, J. J. *J. Phys. Chem. A* **2002**, *106*, 5745.
(35) Varley, D. F.; Levandier, D. J.; Farrar, J. M. *J. Chem. Phys.* **1992**, *96*, 8806.
(36) Siska, P. E. *J. Chem. Phys.* **1973**, *59*, 6052.
(37) Rehfuss, B. D.; Crofton, M. W.; Oka, T. *J. Chem. Phys.* **1986**, *85*, 1785.
(38) Chiang, M. M.; Mahan, B. H.; Maltz, C. *J. Chem. Phys.* **1972**, *57*, 5114.
(39) Baer, M.; Faubel, M.; Martinez-Haya, B.; Rusin, L.; Tappe, U.; Toennies, J. P. *J. Chem. Phys.* **1999**, *110*, 10231.
(40) Baer, M.; Faubel, M.; Martinez-Haya, B.; Rusin, L. Y.; Tappe, U.; Toennies, J. P. *J. Chem. Phys.* **1998**, *108*, 9694.
(41) Faubel, M.; Martinez-Haya, B.; Rusin, L. Y.; Tappe, U.; Toennies, J. P.; Aoiz, F. J.; Banares, L. *J. Phys. Chem. A* **1998**, *102*, 8695.
(42) Rusin, L. Y.; Toennies, J. P. *Phys. Chem. Chem. Phys.* **2000**, *2*, 501.
(43) Polanyi, J. C. *Acc. Chem. Res.* **1972**, *5*, 161.
(44) Sonnenfroh, D. M.; Leone, S. R. *Int. J. Mass Spectrom. Ion Processes* **1987**, *80*, 63.
(45) Liu, D.-K.; Lin, K.-C. *Chem. Phys. Lett.* **1997**, *274*, 37.

JP905610U